Mon. Not. R. Astron. Soc. **000**, 000–000 (0000) Printed 17 September 2014 (MN LATEX style file v2.2)

Deep searches for decameter wavelength pulsed emission from *radio-quiet* gamma-ray pulsars

Yogesh Maan[1,2⋆] and H. A. Aswathappa[1]
[1]*Raman Research Institute, Bangalore 560080, India*
[2]*Joint Astronomy Programme, Indian Institute of Science, Bangalore 560012, India*

arXiv:1409.4434v1 [astro-ph.HE] 15 Sep 2014

ABSTRACT
We report the results of *(a)* extensive follow-up observations of the gamma-ray pulsar J1732−3131 that has been recently detected at decameter wavelengths, and *(b)* deep searches for counterparts of 9 other *radio-quiet* gamma-ray pulsars at 34 MHz, using the Gauribidanur radio telescope. No periodic signal from J1732−3131 could be detected above a detection threshold of 8σ, even with an effective integration time of more than 40 hours. However, the average profile obtained by combining data from several epochs, at a dispersion measure of 15.44 pc cm^{-3}, is found to be consistent with that from the earlier detection of this pulsar at a confidence level of 99.2%. We present this consistency between the two profiles as an evidence that J1732−3131 is a faint radio pulsar with an average flux density of 200–400 mJy at 34 MHz. Detection sensitivity of our deep searches, despite the extremely bright sky background at such low frequencies, is generally comparable to that of higher frequency searches for these pulsars, when scaled using reasonable assumptions about the underlying pulsar spectrum. We provide details of our deep searches, and put stringent upper limits on the decameter wavelength flux densities of several *radio-quiet* gamma-ray pulsars.

Key words: pulsars: general – pulsars: individual: J1732−3131

1 INTRODUCTION

The Large Area Telescope (LAT) on board the *Fermi* gamma-ray satellite, with its unprecedented sensitivity, has revolutionized the study of gamma-ray emitting pulsars, increasing the known population from less than 10 to 121 pulsars[1] (Abdo et al. 2013; Pletsch et al. 2013). About one-third (40) of these pulsars were discovered in blind searches of the LAT data (Abdo et al. 2009; Saz Parkinson et al. 2010; Pletsch et al. 2012b,a,c, 2013). Despite deep searches at frequencies $\gtrsim$ 500 MHz (Saz Parkinson et al. 2010; Ray et al. 2011; Pletsch et al. 2012b), confirmed radio counterparts of only 4 of these have been detected so far (Camilo et al. 2009; Abdo et al. 2010; Pletsch et al. 2012b), suggesting a large fraction of gamma-ray pulsar population to be *radio-quiet*[2].

A likely explanation for the apparent absence of radio emission from the majority of the LAT-discovered pulsars is that their narrow radio beams miss the line of sight towards earth (Brazier & Johnston 1999; Watters & Romani 2011), and hence appear as *radio-quiet*. However, the radio emission beam is expected to become wider at low frequencies (radius-to-frequency mapping in radio pulsars; Cordes 1978), increasing the probability of our line of sight passing through the beam. With this in mind, we used the archival data of the pulsar/transient survey at 34.5 MHz, carried out using the Gauribidanur radio telescope during 2002–2006, to search for decameter-wavelength pulsed emission from several of the LAT-discovered pulsars. A possible detection of radio counterpart of the LAT-discovered pulsar J1732−3131, resulting from the above search, was reported earlier (Maan, Aswathappa, & Deshpande 2012, hereafter Paper I). Weak (and periodic) pulsed emission from J1732−3131 was detected in only one of the several observing sessions. Although scintillation may explain the detection in only one session, another likely possibility is that the radio emission from LAT-discovered pulsars might not be persistent, i.e., they might appear in *radio-bright* mode only once in a while. Two categories of radio pulsars — intermittent pulsars (Kramer et al. 2006) and rotating radio transients (RRATs; McLaughlin et al. 2006) — are well known for such emission behavior.

1.1 Deep search program: motivation

Motivated by the intriguing detection of J1732−3131, we embarked on an observing program of deep searches for the

⋆ E-mail: yogesh@rri.res.in; Current Address: National Centre for Radio Astrophysics, Tata Institute of Fundamental Research, Pune 411007, India.
[1] Additional 28 pulsars detected in gamma-rays are reported to have publications in preparation (Abdo et al. 2013), further increasing the total number of gamma-ray pulsars to 149.
[2] Setting a new convention, the 2$^{\rm nd}$ *Fermi* LAT catalog of gamma-ray pulsars labels all the pulsars with 1.4 GHz flux density $< 30\,\mu$Jy as "radio-quiet". However, as in the usual convention, we use the term radio-quiet only for those pulsars which have no detectable radio flux for an observer at earth.

© 0000 RAS

decameter-wavelength counterparts of the so-called radio-quiet gamma-ray pulsars, using the Gauribidanur radio telescope at 34 MHz. In the first phase of this *deep search program*, each of the target sources in the selected sample of 10 gamma-ray pulsars[3] was observed in multiple (> 20) sessions. *Deep* searches for persistent periodic signals were realized by time-aligning and co-adding the data from these multiple sessions, as described in Section 3. While the significant enhancement in sensitivity achieved this ways is important, the deep search program was motivated by two more crucial factors:

(i) Even for the handful of pulsars which are detectable at such low frequencies, the received periodic signals are very weak. Especially at decameter wavelengths, interstellar and ionospheric scintillation, and contamination from radio frequency interference (RFI), can hinder detection of such weak signals. Hence, a weak source, even if intrinsically persistent, may not be detected in all the observing sessions. In addition, the source may also be intrinsically variable. Hence, it is important to observe the same field multiple times.

(ii) Assuming that our noise statistics are Gaussian, a detection even at 5σ might appear quite significant (chance probability of such a detection is less than 0.6×10^{-6}). But the measured statistics generally deviate from the expected Gaussian nature due to RFI contamination and/or systematics contributed by the receiver, and hence the possibility that a 5σ detection from a single observing session is due to some weak RFI can not be ruled out. However, detection of even a relatively weak periodic signal, but in more than one observing sessions on different days, consistent in pulse-shape and at the same phase of the period, is highly unlikely to be a manifestation of noise (i.e., a chance occurrence) or some RFI. Such consistency across observing sessions, is therefore crucial to raise the level of confidence in establishing the astrophysical origin of an otherwise weak signal.

All the LAT-discovered pulsars which we have searched for, are isolated pulsars with periods in the range 48–444 ms, and only J1813−1246 and J1954+2836 have periods below 100 ms. Among the pulsars for which deep searches have been carried out, J1732−3131 is followed-up most extensively (125 observing sessions). We present here results of our sensitive searches using these follow-ups of J1732−3131 and 9 other pulsars, as well as those using the archival data, and provide useful constraints on the decameter-wavelength flux densities of several radio-quiet gamma-ray pulsars. Section 2 describes details of the archival data and our new observations. In section 3, we explain the search methodologies. Section 4 presents results of follow-up searches of J1732−3131 and several other gamma-ray pulsars, and the upper limits obtained on flux densities of these targets, followed by conclusions in section 5.

2 OBSERVATIONS AND PRE-SEARCH DATA PROCESSING

The archival as well as the new observations were carried out using the Gauribidanur radio telescope. The telescope originally consisted of an array of 640 dipoles (160×4 rows) in the east-west direction (hereafter EW array) and an array of 360 dipoles extending southwards from the center of the EW array (Deshpande, Shevgaonkar, & Sastry 1989). Presently, *only* the EW arm of this telescope is maintained, and the survey as well as the new observations were carried out using this array in coherent phased-array mode. The beam widths of the EW array are 21 arcmin and $25^\circ \times \sec(\mathrm{zenith\ angle})$ in right ascension (RA) and declination (Dec), respectively, with an effective collective area of about $12000\ \mathrm{m}^2$ at the instrumental zenith ($+14^\circ.1$ Dec). The target source is tracked during the observation by steering the phased-array beam electronically. In both sets of observations, data were acquired using the portable pulsar receiver[4] (hereafter PPR; Deshpande, Ramkumar, Chandrasekaran and Vinutha, in preparation) as described in Section 2.3.

2.1 Survey observations

The pulsar/transient survey was carried out in the years 2002–2006 using the EW array at 34.5 MHz, with a bandwidth of 1.05 MHz. The full accessible declination range (-45° to $+75^\circ$) could be covered with 5 discrete pointings in declination: -30°, -05°, $+14^\circ$, $+35^\circ$ and $+55^\circ$. Appropriate pointings were made to cover a large range in right ascension. Apart from J1732−3131, data towards 16 other[5] gamma-ray pulsars are available from single/multiple observing sessions of this survey. Other details of the survey observations towards these sources are given in Table 1.

2.2 New observations

Under the deep search observing program, new observations of 10 radio-quiet gamma-ray pulsars were carried out in multiple sessions spread over several months in 2012. For these observations, a bandwidth of 1.53 MHz centered at 34 MHz was used. Further, these observations could use only 80% of the potential collecting area, since 20% of the EW array dipoles (10% at each of the two far ends) were not available. However, a slightly larger bandwidth and longer session duration, as compared to those of the survey observations, together provided about 18% improvement in sensitivity, despite the 20% loss in the collecting area. Further relevant details of these observations can be found in Table 2. Two radio pulsars, B0834+06 and B1919+21, were also observed regularly as "control pulsars". The position coordinates of the pulsars J0633+0632 and J0633+1746 ([RA,Dec]=[06:34:26, 6.5°] and [06:34:38, 17.8°] respectively, precessed to the epoch of observations) lie close to each other. We observed both of these pulsars simultaneously by pointing towards the direction [06:34:26, 10°.0] (since both the pulsars fall in the same beam, and well above the half power points).

2.3 Data acquisition and pre-search processing

In each of the observing sessions, PPR was used to directly record the raw signal voltage sequence at the Nyquist rate (with 2-bit, 4-level quantization), while tracking the source. In the off-line processing, the voltage time sequence is Fourier transformed in blocks

[3] Our sample also includes J1732−3131, with the aim of making its confirmatory (re-)detection.

[4] `http://www.rri.res.in/~dsp_ral/ppr/ppr_main.html`

[5] Radio counterparts of 3 of these 16 gamma-ray pulsars are known. The radio counterpart of J1907+0602 was reported while our searches were ongoing (Abdo et al. 2010), while those of J1741−2054 and J2032+4127 were already known (Camilo et al. 2009).

of lengths appropriate for a chosen spectral resolution in the resultant dynamic spectrum, and successive raw power-spectra are averaged to achieve desired temporal resolution. For the archival data, appropriate parameters are chosen to achieve 256 spectral channels across 1.05 MHz bandwidth centered around 34.5 MHz, and a temporal resolution of ~ 1.95 ms. For the new observations, the resultant dynamic spectrum consists of 1024 channels across 1.53 MHz bandwidth centered around 34 MHz, with a temporal resolution of ~ 2 ms.

To identify RFI contaminated parts of the data, *robust*[6] mean and standard deviation are computed, and an appropriate threshold in signal-to-noise ratio (S/N) is used separately in the frequency and time domains. First the RFI contaminated frequency channels are identified, and data from these channels are excluded while identifying the time samples contaminated with RFI. The RFI contaminated frequency channels as well as time samples are excluded from any further processing. Most of the observations were conducted in the night time, and typically only a few percent ($< 5\%$) of the data were found to be RFI contaminated. From the new observations, time-intervals cumulating to about one observing session duration were rejected for J0633+0632/J0633+1746 and J1809−2332. Several of the observing sessions towards J1732−3131 happened to be in the day time, and only 85 sessions worth of effective integration time could be used out of a total of 125 observing sessions.

3 SEARCH METHODS AND SENSITIVITY

The individual observing session data were searched for presence of single bright pulses as well as for pulsed signals at the expected periods of the respective gamma-ray pulsars. While the detailed methodologies of these two kinds of searches can be found in Maan (2014) and Section 2 of Paper I, a brief overview is provided below.

3.1 Single pulse search

Searching for bright single pulses involves dedispersing the data at a number of trial dispersion measures (DM), and subjecting the individual time series, corresponding to each of the trial DMs, to a common detection criterion, i.e. an appropriate S/N threshold. For optimum detections, the individual time series are systematically smoothed with a template of varying width, effectively carrying out a search across the pulse-width as well. We sample the template width range in a logarithmic manner, with a step of 2 (i.e., we use 2^n time-samples wide templates, where n varies from 0 to a maximum chosen value, in steps of 1)[7]. We carried out the single pulse search in two different ranges of DMs: 0–20 pc cm^{-3} and 20–50 pc cm^{-3}, with the consecutive trial DMs in the two ranges differing by 0.01 pc cm^{-3} and 0.05 pc cm^{-3}, respectively. The maximum match filter widths used for the two ranges are 128 ms and 256 ms, respectively. The S/N threshold is chosen based on how many "false alarms" can be tolerated in the final candidate list. For N_{tot} number of points in a time series, the expected number of "false-alarms", N_f, crossing a threshold of η (in units of the rms noise) solely due to noise, are given by:

$$erf(\eta/1.414) = 1 - 2 \times N_f/N_{tot} \quad (1)$$

where $erf()$ is the *error function*. Allowing 5 false alarms from each of the trial DMs[8], implies a S/N threshold less than 5. Note that scaling-up of the denominator on the right-hand side of Eq. 1 appropriately, so as to account for the number of trial widths as well, does not make the implied threshold significantly different from 5. So, we have used a detection threshold of 5 in our single pulse searches. However, detections marginally above this threshold can be confirmed only when reasonable number of single pulses are detected at the same DM. In case of detection of a single bright pulse, we need to insist on larger S/N ($\geqslant 8$), so that consistency as well as the dispersive nature of the signal can be checked across the bandwidth.

3.2 Search for dispersed periodic pulses

The periodicity search using data from individual observing sessions involves folding the time series corresponding to each of the frequency channels over the expected period of the respective gamma-ray pulsars. The *folded dynamic spectrum* is then used to search for a dispersed signal, in a way similar to that used in the deep searches for dispersed periodic pulses described below (Section 3.3). We also search over a narrow range of period offsets around the expected period. Extending the search in the period-domain is particularly important for the archival data, since the observation epoch is well before the launch of the Fermi mission and the validity of the back-projected gamma-ray ephemeris can not be ensured. For the parameters of our search, the optimum S/N threshold, as suggested by Lorimer & Kramer (2004), is about 5. However, we set a slightly higher S/N threshold of 8 to account for any low level RFI, as well as to be able to check for consistency of a signal across the observation bandwidth.

The multiple observing sessions towards each of the target sources allowed us to explore any transient or non-persistent periodic emission from these pulsars. The multiple session data from the new observations were used to carry out deep searches, details of which are given below.

3.3 Deep search for dispersed periodic pulses

Since the rotation ephemerides for the gamma-ray pulsars are known from timing of the LAT data[9], multiple session data from the new observations could be used advantageously to enhance our sensitivity for detecting a periodic signal. For each of our target gamma-ray pulsars, we use the pulsar timing software TEMPO[10] along with the corresponding timing model, to predict the pulsar

[6] It is possible that the computed mean and standard deviation get biased by a few very strong pulses. To get an unbiased (or robust) estimate, mean and standard deviation are recalculated by using the previous estimates to detect and exclude the strong pulses above a given S/N threshold. This process is continued iteratively till the computed mean and standard deviation no more differ from their respective values in the previous iteration.

[7] As evident from Eq. 2, for a given peak flux density, the highest achievable S/N of a pulse is directly proportional to square-root of its width. Hence, for an optimum width-search, we sample the trial pulse width range in a logarithmic manner.

[8] Our choice of tolerable number of false alarms is admittedly large, to increase the probability of detecting the faint pulses.

[9] The up-to-date timing models of several gamma-ray pulsars are provided by the LAT team at `https://confluence.slac.stanford.edu/display/GLAMCOG/LAT+Gamma-ray+Pulsar+Timing+Models`

[10] For more information about TEMPO, please refer to the website: `http://www.atnf.csiro.au/research/pulsar/tempo/`.

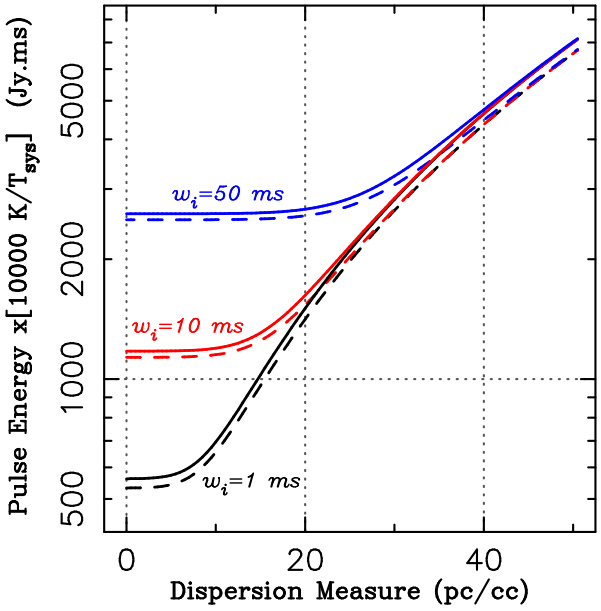

Figure 1. The minimum detectable pulse energies, normalized by T_{sys} in units of 10000 K, for intrinsic pulse widths of 1, 10 and 50 ms (the lower, middle and upper pairs of curves, respectively), are shown as functions of DM. The solid and dashed curves correspond to the new observations and the archival data, respectively. For pulses with intrinsic widths smaller than 2 ms, the observed pulse width is limited by our sampling time ($\sim$ 2 ms), and the corresponding sensitivity curves will nearly follow that for w_i = 1 ms. Scatter broadening dependence on DM as modelled by Bhat et al. (2004), and the collecting area corresponding to a pointing declination at the instrumental zenith has been used.

period and the pulse phase. The dynamic spectrum for each of the observing sessions is folded over the predicted pulse period (the time-ranges identified as RFI-contaminated in the pre-search processing are excluded). The *folded dynamic spectra* from all the observing sessions of a particular source are then phase-aligned and co-added. While co-adding, the average band-shape modulation is removed, and the frequency channels identified as RFI contaminated in individual observing sessions are excluded. Also, to account for possible differences in the effective integration time of individual sessions (i.e., the RFI-free observation duration), a suitably weighted average of the folded dynamic spectra is computed.

To search for a dispersed signal, the final co-added (or more precisely, *averaged*) folded dynamic spectrum is dedispersed for a number of trial dispersion measures, and the significance of the resultant average profiles is assessed. To enhance the signal-to-noise ratio (S/N), the profiles are smoothed to a resolution of about 20° to 30° in pulse-longitude, and sum-of-squares (Paper I) or χ^2 (Leahy et al. 1983) is used as the figure of merit to assess the profile significance. An in-house developed software pipeline was used to perform the above search. The pipeline was successfully verified using observations of our control pulsars.

3.4 Single pulse search sensitivity

In our single-pulse searches, the peak flux density of a temporally resolved pulse (Cordes & McLaughlin 2003), is given by:

$$S^{\rm SP}_{\rm peak} = (S/N)_{\rm peak} \times \frac{2k_B T_{sys}}{A_e(z)\sqrt{n_p\, W\, \Delta\nu}} \qquad (2)$$

where, $T_{\rm sys}$ is the system temperature, $A_e(z)$ is the effective collecting area as a function of zenith-angle (z), $\Delta\nu$ is the observation bandwidth, n_p is the number of polarizations (1 for Gauribidanur telescope), and $(S/N)_{\rm peak}$ is peak signal-to-noise ratio of the pulse corresponding to a smoothing optimum for its observed width of W.

Note that the observed pulse width is contributed to by various pulse broadening effects, viz. intrinsic pulse width, interstellar scattering, receiver filter response time, and residual dispersion smearing across individual frequency channels. However, the scatter broadening at such low frequencies dominates over other pulse broadening effects even for moderate values of DM. Hence, at moderately high DMs, sensitivity of our single pulse search, in terms of pulse energy (i.e., $S^{\rm SP}_{\rm peak} \times W$), becomes independent of the *intrinsic* pulse width. This is clearly seen in Figure 1 which shows the minimum detectable pulse energy for intrinsic pulse widths of 1, 10 and 50 ms, as a function of DM. For instance, beyond a DM of about 25 pc cm^{-3}, the minimum detectable pulse energy for all the pulses with intrinsic widths $\leqslant$ 10 ms is same. We have followed the scatter broadening dependence on DM as modelled by Bhat et al. (2004). Also, we have used the collecting area corresponding to a pointing declination at or near the instrumental zenith of $14^\circ.1$. For a declination away from zenith, the sensitivity will decrease by a factor of $\sec(z)$.

3.5 Periodic signal search sensitivity

For periodicity searches, the minimum detectable flux density $S^{\rm P0}_{\rm min}$, i.e., at the threshold signal-to-noise ratio $(S/N)_{\rm min}$, is given by (Vivekanand, Narayan, & Radhakrishnan 1982):

$$S^{\rm P0}_{\rm min} = (S/N)_{\rm min} \times \frac{2k_B T_{\rm sys}}{A_e(z)\sqrt{n_p\, t_{\rm obs}\, \Delta\nu}} \sqrt{\frac{W}{P-W}} \qquad (3)$$

where, W is the pulse width, P is the pulse period and $t_{\rm obs}$ is the total integration time. For archival data, $t_{\rm obs}$ is equal to the total observation duration of a single session (i.e., about 1200 s). For new observations, $t_{\rm obs}$ equals the cumulative observation duration of all the sessions.

4 RESULTS AND DISCUSSION

4.1 Searches using the archival data

Our searches for bright single pulses as well as for periodic signals using the archival data did not result in any further detection of decameter-wavelength counterparts of radio-quiet gamma-ray pulsars. For the archival data, the upper flux density limits for periodic as well as single pulse emission are presented in Table 1. To enable easy comparison with the flux density limits at higher radio frequencies available in literature, generally computed for a detection limit of $5\,\sigma$, the upper limits presented in Table 1 are also computed for a $(S/N)_{\rm min}$ of 5. For the archival observations, our target sources were generally offset from the pointing center of the beam. To calculate the factor by which the gain reduces at the target source declination, relative to the beam-center declination, we assume a theoretical beam-gain pattern: $P(\theta) = [\sin(\pi D \sin\theta/\lambda)/(\pi D \sin\theta/\lambda)]^2$, where $D = 20$ m and $\lambda = 8.8$ m. The flux density limits estimated at the beam center are then scaled-up using the above correction factors computed for re-

Table 1. Searches using the archival data: Observation details and upper flux density limits.

Sr. No.	Target PSR	Pointing Dec. (°)	Pointing offset (°)	t_{obs} (s) $[N_{\rm sessions} \times \tau]$	$T_{\rm sky}$ (K)	$S^{\rm SP}_{\rm min}$ (Jy)	$S^{\rm P0}_{\rm min}$ (mJy)
1	J0357+3205	+35	3	2×1200	18100	72	218
2	J0633+0632	+14	7	1×1200	19900	91	278
3	J0633+1746	+14	4	1×1200	19900	77	234
4	J1741−2054	−30	9	1×1200	62600	386	1174
5	J1809−2332	−30	6	3×1200	62400	340	1036
6	J1813−1246	−05	8	4×1200	76000	387	1179
7	J1826−1256	−05	8	3×1200	80100	408	1242
8	J1846+0919	+14	5	1×1200	62900	254	774
9	J1907+0602	+14	8	1×1200	71700	357	1087
10	J1954+2836	+35	6	2×1200	45000	202	614
11	J1957+5033	+55	4	1×1200	35300	173	527
12	J1958+2846	+35	6	2×1200	47100	211	642
13	J2021+4026	+35	5	4×1200	43200	184	560
14	J2032+4127	+35	6	2×1200	38200	171	521
15	J2055+2539	+35	9	2×1200	35900	199	605
16	J2238+5903	+55	4	1×1200	28100	138	420

Notes. — (1) "Pointing offset" is the difference between the pointing declination and the true declination of the target pulsar. (2) Since the computation of sensitivity limits do not take into account any possible offset in RA, the limits in some cases might be underestimated, at most (i.e., in the worst case) by a factor of 2. (3) τ is the individual observing session duration, and t_{obs} is the total observation duration of all the sessions towards a particular source.

Table 2. Deep searches: Observation details, and comparison of upper flux density limits with those from earlier searches.

Sr.	Target PSR	t_{obs} (s)	$T_{\rm sky}$	$S^{\rm SP}_{\rm min}$	$S^{\rm P0}_{\rm min}$	Comparison with searches at higher frequencies				
No.		$[N_{\rm sessions} \times \tau]$	(K)	(Jy)	(mJy)	$S_{\rm previous}$ (mJy)	$\nu_{\rm obs}$ (MHz)	Ref.	$S^{\rm Scaled}_{\rm previous}$ (μJy)	$S^{\rm P0,Scaled}_{\rm min}$ (μJy)
1	J0357+3205	24×1800	17200	67	34	0.043	327	c	2	20
2	J0633+0632†	45×1800	19900	77	28	0.075	327	c	4	17
3	J0633+1746†	45×1800	19900	102	38	150.0	35	a	94	22
4	J1732−3131‡	85×1800	51400	271	73	0.059	1374	c	57	43
5	J1809−2332	20×1800	74900	348	193	0.026	1352	c	24	114
6	J1836+5925	33×1800	24700	128	55	0.070	350	c	4	32
7	J2021+4026	24×1800	44100	181	92	0.051	820	c	17	54
8	J2055+2539	22×1800	30400	114	60	0.085	327	b	5	35
9	J2139+4716	23×1800	32500	143	74	0.171	350	d	11	44
10	J2238+5903	22×1800	29700	154	82	0.027	820	c	9	48

$N_{\rm sessions}$ is modified (lowered) so that t_{obs} provides the *effective* integration time (i.e., the integration time after excluding the RFI contaminated time intervals).

† The upper flux density limits presented for these pulsars are modified by the correction factors for the respective offsets from the pointing declination.

‡ Using a pulse duty cycle of 50% (instead of 10%) for J1732−3131, as indicated by its average profile, would increase the corresponding $S^{\rm P0}_{\rm min}$ by a factor of 3.

References — (a) Ramachandran et al. 1998; (b) Saz Parkinson et al. 2010; (c) Ray et al. 2011; (d) Pletsch et al. 2012b.

spective source position offsets[11]. Note that we have carried out the above correction only for the offsets in declination. Possible offsets in RA are less than 1 minute (i.e., above the half-power points in the beam-gain pattern). Whenever archival data are available from multiple sessions, the offsets in RA are different for different sessions, and generally the RA offset is negligible at least for one of the sessions. Hence, Table 1 presents the sensitivity limits for the best case when there is no offset in RA, and the limits in some cases might be underestimated, at most (i.e., in the worst case) by a factor of 2. The sensitivity limits for the single pulse search ($S^{\rm SP}_{\rm min}$) are computed for a nominal pulse width of 100 ms, while those for the periodicity search ($S^{\rm P0}_{\rm min}$) are computed for a pulse duty cycle of 10% and observation-duration of a single observing session, i.e., 1200 s.

[11] As explained in Paper-I, system temperature at the beam center is estimated by computing a weighted average of sky temperature estimates (Dwarakanath & Udaya Shankar 1990) at several points across the large beam using a theoretical beam-gain pattern.

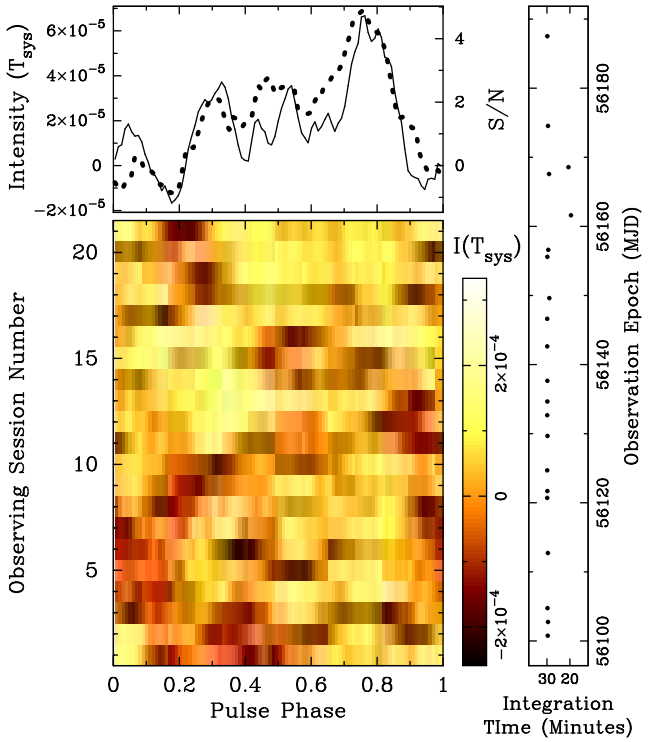

Figure 2. Rows in the color image show phase-aligned average profiles of J1732−3131 observed at different epochs (arranged in ascending order of epoch). The upper panel shows the net average profile (solid line) and the average profile from our earlier detection using the archival data (dotted line; see Paper I), for ready comparison. The intensity range of the latter profile is normalized to that of the former. All the individual profiles in the color image as well as the two profiles in the upper panel are smoothed by a 45° wide window. For the observing sessions corresponding to different rows in the main panel, the side panel shows the epochs of observation and the effective integration time (earliest epoch corresponds to first observing session). Although it is not readily apparent in this figure due to low S/N, the profile shape is consistent across the complete range of observing session number, i.e., the net average profile has a nearly uniform contribution from all the sessions (see a moving average filtered version of the color image in Figure S1).

4.2 Deep follow-up observations of J1732−3131

We carried out extensive follow-up observations of J1732−3131, distributed in 125 sessions, amounting to a total of 62.5 hours of observation time. In our deep search using an effective integration time of about 42.5 hours (after rejecting the RFI contaminated time sections), we could not (re-)detect any readily apparent (i.e., above a detection threshold of 8σ) periodic signal from J1732−3131. Our searches for single bright pulses as well as for periodic signal using the individual session data also did not result in any significant candidate above our detection threshold of 8σ.

Although we did not have any significant detection, the possibility of a signal weaker than our detection threshold can not be ruled out. Since we have an estimate of the DM from our candidate detection of this pulsar (15.44 ± 0.32 pc cm^{-3}; Paper I), we can look for weak periodic signals at this DM that are consistent over multiple observing sessions. Furthermore, allowing for the possibility that the periodic signal might be very weak, if at all present, we carefully chose the observing sessions that are virtually free from RFI contamination (assessed by visual inspection of the dynamic spectrum), and where the dedispersed folded profiles were found to have full-swing S/N (i.e., peak-to-peak S/N) more than 4. Such average profiles, corresponding to 21 sessions, are phase-aligned and presented in Figure 2. For comparison, we have overlaid the average profile from the original detection (dotted line; hereafter *the old profile*) on the net average profile of all the 21 sessions (solid line; hereafter *the new profile*) in the upper panel. The two profiles are manually aligned, since accuracy of the time-stamp in the archival data is not adequate enough. The two profiles, observed 10 years apart, exhibit striking similarity, and both are consistent with each other within the noise uncertainties. As a quantitative measure of the similarity, the Pearson (normalized) correlation coefficient between the two profiles is found to be 0.85.

To further assess statistical significance of the apparent similarity between the two profiles, we performed Monte-Carlo simulation. An individual realization in our simulation involves generating a random noise profile and finding its cross-correlation with the old profile. To be compatible with the smoothed profiles shown in Figure 2, the random noise profile is also smoothed with a 45° wide window. The resultant noise profile is cross-correlated with the old profile at all possible phase-shifts, and the maximum (normalized) correlation coefficient is noted down. We simulated 10 million such independent realizations. The maximum correlation coefficient was found to be $\geqslant 0.85$ (i.e., equal to or greater than the correlation found between the old and the new profile) only in 0.8% of these realizations. Hence, the probability of the old and the new profiles having the same origin is estimated to be 0.992. In other words, the two profiles are consistent with each other at a confidence level of 99.2%.

The observed consistency between the average profile shape obtained by combining data from multiple epochs and that from the original detection 10 years ago, compels us to infer that (a) our candidate detection (Paper I) was not a mere manifestation of noise or RFI, and hence (b) the LAT-pulsar J1732−3131 is not radio-quiet. If true, the dispersion measure of this pulsar is 15.44 ± 0.32 pc cm^{-3} (Paper I). Also, our earlier estimate of the average flux density (i.e., pulse-energy/period) of this pulsar in Paper I (~ 4 Jy; at 34.5 MHz) was most probably affected by scintillation. The new average profile provides a better estimate (since the scintillation effects are expected to average out), and suggests the average flux density to be 200–400 mJy at 34 MHz. With this new estimate, non-detection of this pulsar at higher radio frequencies could be explained with a spectral index $\lesssim -2.3$, assuming no turn-over (Izvekova et al. 1981) in the spectrum. This upper limit on the spectral index lies on the steeper edge of the range of spectral indices for normal pulsars (-1.4 ± 1.0; Bates, Lorimer & Verbiest 2013).

4.3 New observations towards other target sources

In a couple of observing sessions towards the telescope pointing direction of RA=06:34:26, Dec=10°, we detected a few ultra-bright pulses at two different DMs of about 2 pc cm^{-3} and 3.3 pc cm^{-3}, respectively. However, when dedispersed at the DMs suggested by the bright single pulses, no significant signal was found at the expected periodicities of our target pulsars J0633+0632 and J0633+1746, which would have been in the telescope beam centered at above coordinates. Energies of these strong pulses in the two observing sessions are comparable to typical energies of giant pulses from the Crab pulsar at decameter wavelengths (Popov et al. 2006). More detailed investigations of these single pulses will be reported elsewhere.

No significant pulsed (periodic or transient) signal, above a

detection threshold of 8σ, was found towards the directions of other selected gamma-ray pulsars. The upper limits on corresponding flux densities, for a detection limit[12] of 5σ, are presented in Table 2. For computing the periodic signal search sensitivity ($S_{\rm min}^{\rm P0}$), we have excluded the time-intervals rejected as RFI contaminated from the total integration time. To compare with the earlier searches at higher frequencies, we have also compiled the flux density limits ($S_{\rm previous}$) from literature, along with their corresponding observation frequencies ($\nu_{\rm obs}$), in Table 2. In case of the limits being available at several frequencies, the one at the lowest frequency (i.e., closest to 34 MHz) has been used. Wherever needed, these limits were scaled to 5σ-level, before compiling into the table. For comparison, our limits at decameter wavelengths and those from literature are scaled to 1.4 GHz using a spectral index of -2.0, and presented as $S_{\rm min}^{\rm P0,Scaled}\left(= S_{\rm min}^{\rm P0} \times \left[\frac{1400}{34}\right]^{-2}\right)$ and $S_{\rm previous}^{\rm Scaled}\left(= S_{\rm previous} \times \left[\frac{1400}{\nu_{\rm obs}}\right]^{-2}\right)$, respectively. We have assumed that there is no spectral turn-over above our observation frequency (i.e., 34 MHz). Note that Bates, Lorimer & Verbiest (2013) and Maron et al. (2000) have estimated the average spectral index for normal pulsars to be -1.4 ± 1.0 and -1.8 ± 0.2, respectively. Our assumed spectral index (i.e., -2.0), although lying on the steeper side, is well consistent with both these estimates. Despite the large background sky-temperature at our observing frequency, for a couple of pulsars our flux density limits are better than those from deep searches at higher radio frequencies, and in other cases they are only within a factor of few of the limits from shorter wavelength searches (provided the spectral index of these sources is equal to or steeper than -2.0).

The above comparison of flux density limits may appear to be optimistic, since we have not assumed any turn-over in the spectrum. However, even with a turn-over around 80–100 MHz, our flux density limits scale to typically a few hundreds of μJy at 1.4 GHz. Further, if the lack of radio emission from the LAT-discovered pulsars is indeed due to unfavorable viewing geometries, then the pulsars which could possibly be detected at decameter wavelengths can be expected to have steep spectra. If we assume a fairly steep spectrum with an index of -3.0 (for comparison, the spectral index of B0943+10 is -3.7 ± 0.36; Maron et al. 2000), most of our flux limits scale to less than 100μJy at 1.4 GHz, and some of them are still comparable to those reported at higher frequencies.

The possibility that some of our target sources are "radio-loud", but have flux densities below our detection limits, can not be ruled out. The very faint radio emission from J1732−3131 which could be assessed only by making use of its DM estimated from earlier detection (Paper I), indicates the possibility of very faint emission from a few more of the (so far) *radio-quiet* gamma-ray pulsars. However, lack of radio detection from most of our target sources indicates that a large fraction of our sample may indeed be radio-quiet. Consequently, the high fraction of gamma-ray pulsars being radio-quiet is consistent with the predictions of "narrow polar-cap" models (e.g., Sturrock 1971; Ruderman & Sutherland 1975) for radio beams and "fan-beam outer magnetosphere" models (e.g., Romani 1996) for gamma-ray emission.

[12] As mentioned earlier, the flux density limits are computed for a $(\rm S/N)_{\rm min}$ of 5, to enable easy comparison with the flux density limits at higher radio frequencies available in literature.

5 CONCLUSIONS

The following points summarize the results of our deep searches for decameter wavelength counterparts of several *radio-quiet* gamma-ray pulsars:

(i) We have shown that the 34 MHz average profile of the LAT-discovered pulsar J1732−3131 obtained by effectively integrating over more than 10 hours of new observations carried out at different epochs (Figure 2) is consistent with that from the first radio detection of this pulsar (Maan, Aswathappa & Deshpande 2012) at a confidence level of 99.2%. We present this consistency as an evidence that J1732−3131 is a faint radio pulsar *(and not radio-quiet)* at decameter wavelengths.

(ii) We have put stringent upper limits on pulsed (transient as well as periodic signal) radio emission from several of the radio-quiet gamma-ray pulsars at decameter wavelengths (Table 2). Despite the extremely bright sky background at decameter wavelengths, the flux density limits obtained from our deep searches are comparable to those from higher frequency searches of these pulsars, when scaled to 1.4 GHz assuming a spectral index of -2.0 and no turn-over in the spectrum.

We would also like to emphasize that in the process of carrying out the deep searches, the Gauribidanur radio telescope is now appropriately equipped with a sensitive setup to detect and study known periodic signals with average flux densities as low as a few mJy, even at such low frequencies.

ACKNOWLEDGMENTS

We gratefully acknowledge the support from the observatory staff. We thank the anonymous referee for a critical review of our manuscript, as well as for the comments and suggestions which helped in improving the manuscript. YM is thankful to Avinash Deshpande for useful discussions and comments on the manuscript. YM is grateful to Paul Ray and other members of the LAT-team for providing the up-to-date timing models of several gamma-ray pulsars. We gratefully thank Indrajit V. Barve, Hariharan K., Rajalingam M., and several other colleagues, for their help with the observations at several occasions. The Gauribidanur radio telescope is jointly operated by the Raman Research Institute and the Indian Institute of Astrophysics.

REFERENCES

Abdo A. A. et al., 2009, Science, 325, 840
Abdo A. A. et al., 2010, ApJ, 711, 64
Abdo A. A. et al., 2013, ApJS, 208, 17
Bates S. D., Lorimer D. R., Verbiest J. P. W., 2013, MNRAS, 431, 1352
Bhat N. D. R., Cordes J. M., Camilo F., Nice D. J., Lorimer D. R., 2004, ApJ, 605, 759
Brazier K. T. S., Johnston S., 1999, MNRAS, 305, 671
Camilo F. et al., 2009, ApJ, 705, 1
Cordes J. M., 1978, ApJ, 222, 1006
Cordes J. M., McLaughlin M. A., 2003, ApJ, 596, 1142
Deshpande A. A., Shevgaonkar R. K., Sastry C. V., 1989, J.IETE, 35, 342
Dwarakanath K. S., Udaya Shankar N., 1990, Journal of Astrophysics and Astronomy, 11, 323

Izvekova V. A., Kuzmin A. D., Malofeev V. M., Shitov I. P., 1981, Ap&SS, 78, 45
Kramer M., Lyne A. G., O'Brien J. T., Jordan C. A., Lorimer D. R., 2006, Science, 312, 549
Leahy D. A., Darbro W., Elsner R. F., Weisskopf M. C., Kahn S., Sutherland P. G., Grindlay J. E., 1983, ApJ, 266, 160
Lorimer D. R., Kramer M., 2004, Handbook of Pulsar Astronomy, Ellis R., Huchra J., Kahn S., Rieke G., Stetson P. B., eds.
Maan Y., 2014, PhD thesis, Indian Institute of Science, Bangalore, `http://hdl.handle.net/2289/5908`
Maan Y., Aswathappa H. A., Deshpande A. A., 2012, MNRAS, 425, 2
Maron O., Kijak J., Kramer M., Wielebinski R., 2000, A&AS, 147, 195
McLaughlin M. A. et al., 2006, Nature, 439, 817
Pletsch H. J. et al., 2013, ApJ, 779, L11
Pletsch H. J. et al., 2012a, ApJ, 755, L20
Pletsch H. J. et al., 2012b, ApJ, 744, 105
Pletsch H. J. et al., 2012c, Science, 338, 1314
Popov M. V. et al., 2006, Astronomy Reports, 50, 562
Ray P. S. et al., 2011, ApJS, 194, 17
Romani R. W., 1996, ApJ, 470, 469
Ruderman M. A., Sutherland P. G., 1975, ApJ, 196, 51
Saz Parkinson P. M. et al., 2010, ApJ, 725, 571
Sturrock P. A., 1971, ApJ, 164, 529
Vivekanand M., Narayan R., Radhakrishnan V., 1982, Journal of Astrophysics and Astronomy, 3, 237
Watters K. P., Romani R. W., 2011, ApJ, 727, 123

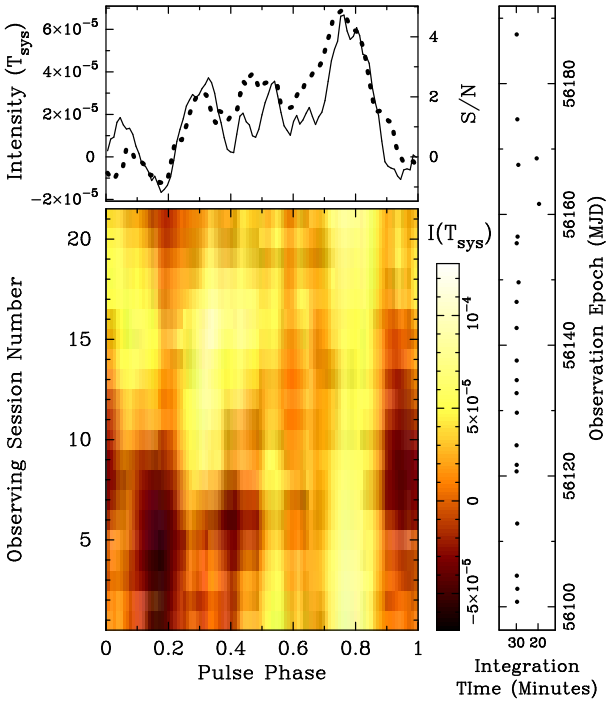

Figure S1. Same as Figure 2 in the main paper, except that each row in the color image now represents an average profile obtained from 11 observing sessions — an average of profiles from ± 5 sessions around the session corresponding to the row. For example, the profile corresponding to session number 15 represents an average of profiles from the sessions in the session number range 10–20. Note that, at the edges of the session number range, the moving average filter is wrapped around. For example, the $20^{\rm th}$ row profile corresponds to an average of profiles from the sessions in the ranges 15–21 and 1–4. Note that all the 4 components (at pulse phases ~ 0.8, ~ 0.55, ~ 0.3, and ~ 0.08) exhibit consistency across the observing sessions, with the brightest component at pulse phase ~ 0.8 *appearing* to be, as expected, most consistent.